


# Adherence and Failure of an EBPVD 7YSZ Coating on a $\beta/\gamma$ -NiCrAl Substrate: A Pilot Study

Klaus Fritscher<sup>1</sup>  · Claus-Jürgen Kröder<sup>1</sup> · Uwe Schulz<sup>1</sup>

Received: 10 April 2016 / Revised: 28 June 2016 / Published online: 18 July 2016  
© Springer Science+Business Media New York 2016

**Abstract** Oxidation, lifetime and crack path at failure upon furnace oxidation testing at 1100 °C were evaluated for an undoped alumina-forming NiCrAl alloy/7YSZ (7 wt% yttria stabilized zirconia) coating system. The coating was deposited by electron beam physical vapor deposition (EBPVD). The thermally grown oxide (TGO) was investigated by energy dispersive spectroscopy. The outer zone of the TGO comprised a particular interlayer-denominated mixed zone (MZ), which revealed accumulation of Cr together with Y and Zr. The contents of Y and Zr in the MZ of the undoped sample were in good agreement with compositional data previously evaluated for thermal barrier coating (TBC) systems with EBPVD NiCo-CrAlY bond coats versus relative lifetime. These data are considered characteristic measures of the stage of life for EBPVD TBC systems.

**Keywords** Electron beam physical vapor deposition · EBPVD thermal barrier coating · TBC adherence · TBC lifetime · Thermally grown oxide

## Introduction

Typical thermal barrier coating systems (TBCs) are ceramic top coats of 7 wt% yttria stabilized zirconia (7YSZ) applied on bond coated superalloy segments operating in the hot sections of gas turbines. The YSZ ceramic is deposited by means of air plasma spraying (APS) or reactive electron beam physical vapor deposition (EBPVD). The bond coats below the topcoat are alumina-forming interlayers. They are applied either by PtAl in-diffusion generating  $\beta$ -NiPtAl rich phases or MCrAlY (M: Ni and/or Co) overlay deposition resulting in a random  $\beta/\gamma$ -phase structure. The overlay bond coats are mostly applied via a low pressure

---

✉ Klaus Fritscher  
klaus.fritscher@goettersiedlung.de

<sup>1</sup> Institute of Materials Research, DLR-German Aerospace Center, 51170 Cologne, Germany

plasma spray process or to a lesser extent by EBPVD. The same holds for the PS- and PVD-based ceramic topcoats.

During high temperature exposure, the bond coat forms a thermally grown oxide layer (TGO) by ingress of oxygen through the YSZ topcoat—this applies equally to both PS and PVD topcoats—from the external atmosphere, selective Al outward diffusion from the metal to the metal/YSZ interface, and interaction of the growing scale with the YSZ topcoat. The process of interaction creates a particular interlayer at the upper TGO termed “mixed zone” (MZ) [1–3]. It basically consists of a fine-grained alumina matrix with embedded  $ZrO_2$  dispersion.

To avoid misunderstanding in the characterization of PS- and PVD-based TBCs, substantial differences between the two types of TBC systems must be settled. In fact, they differ in some details essentially [4]. The variances in properties and characteristics are related to the gas content solved in the bond coat, the pretreatments prior to coating, and the impact of physical and geometrical specifications on lifetime and failure. Following distinctive features are given in detail:

1. EBPVD bond coats have an oxygen content of <10 ppm only which is about two orders of magnitude less than for the PS bond coat versions.
2. The deposition of metallic and ceramic coatings on substrates and bond coats via plasma spraying requires rough and jagged surfaces which is favorably provided by grit-blasting. Preceding “grit-blast-cleaning” of EBPVD TBC systems, however, resulted in shorter furnace cycle lives [5]. Moreover, exceptional smooth and flat surfaces (4000 grit finish) of the substrates prior to EBPVD deposition doubled the life compared to the standard systems [6].
3. The sites of failure on thermal fatigue of PS systems can encompass the whole TGO and even parts of the TBC (spots of “white failure”). They normally show a serrated multiple fracture mode. In the corresponding PVD TBC systems (definitely for Hf-free NiCoCrAlY bond coated Hf-free substrates), they exclusively fail in a plain manner along the bond coat/scale interface.
4. The impact of TBC thickness on the lifetime is significant for PS versions: minor lifetimes for TBCs having thicker PS top coats are reported [4]. On the other hand, a corresponding effect for EBPVD TBC systems has been ruled out [1].
5. More frequent fast temperature cycles of PS systems shorten the lifetimes (=less hot hours) [4]. The life of the PVD-type systems, however, is independent on the number of thermal cycles. It depends on the time at service temperature only [2]. A particularly rapid cycle frequency of 10-min cycles with holding for 5 min at 1100 °C, however, even increased the lives of EBPVD TBCs with NiCoCrAlY bond coats [4].
6. The CTE mismatch between metal base and the TGO is commonly considered a highly critical value, e.g., when calculating lifetime predictions. A rather complex stress distribution in particular convex areas, e.g., of turbine blades has been specified as described in the literature over the last decades. This view is primarily based on numerous lifetime results obtained with PS coated TBC systems [7]. In the case of EBPVD layers, however, the lifetimes are obviously

independent of the CTE mismatch [1, 8]. This point is taken up again in the “Causes of Failure and Failure Mechanisms Of EBPVD TBC Systems” section.

Some features concerning lifetime and failure depend on stresses that build up between the layers. This is particularly true for the aspects of the points 4, 5 and 6, namely for the PS variants. A corresponding dependence of these properties is not observed in the alternative PVD systems. In the case of PVD systems, it is thereby possible to focus on problems of adhesion and life without considering mechanical interlocking at interfaces and additional stress phenomena. These issues are addressed in points 2 and 3.

The adhesion of the layers in EBPVD TBC composites ends due to thermal fatigue resulting in separation along the scale/ $\gamma$ -Ni interphase. Except for  $\gamma$ -Ni, all other Al-containing metal phases have been consumed via selective oxidation of Al during the typical long lifetimes of TBC systems at temperature. So, if the adhesion between scale and metal is to be examined by a TBC model system, the system must meet the following characteristics:

- (i) a short maximum lifetime thus restricting the selective oxidation of Al,
- (ii) a sufficient size of the Al-containing phases to co-exist throughout the life,
- (iii) a controlled shape and alignment of the phases to maintain constant geometric ratios between the phases during the entire life.

In this paper, it is attempted to meet these characteristics. An undoped NiCrAl alloy substrate of ternary eutectic composition will be provided in the directionally solidified (DS) state [9]. It will be used as a surrogate EBPVD bond coat. It solidifies to a lamellar composite of  $\beta$ -NiAl,  $\gamma$ -Ni and  $\alpha$ -Cr phase. Upon which a YSZ top coat will be deposited by EBPVD. So the respective metal phase of the substrate offers the opportunity to discover differences in the adhesion strength on furnace testing between these phases and the TGO on top of them jointly. The work complements a previous study on PVD TBC systems with MCrAlY bond coats [8]. It provides further insight on the nature of adhesion and the lifetime of TBC systems.

## Experimental Procedures

### Provision of Material for Furnace Testing

The following high purity elemental charge material was supplied by GfE for the manufacture of particular substrates. It is basically devoid of traces of quickly segregating elements like sulfur, carbon, and phosphorus:

Al rods > 99.99 %

Ni pellets > 99.9 %

Cr flakes > 99.7 %

By means of this material, a Ni–37.5Cr–7Al wt% alloy rod was produced via two-stage induction melting in 99.7 % purity corundum crucible under a hydrogen atmosphere and subsequent vacuum and cast in a rotating copper mold, followed by Bridgman-type directional solidification processing [10]. The ternary eutectic melts at 1302 °C. On unidirectional solidification, three phases crystallize simultaneously to an aligned lamellar structure of  $\alpha$ -Cr,  $\beta$ -NiAl, and  $\gamma$ -Ni, as shown in Fig. 1. The compositions of the phases are given in Table 1. The interlamellar spacing is about 12  $\mu\text{m}$ .

The as-solidified alloy represents the metastable state of the alloy (Fig. 1); the high temperature phases are frozen in. Under equilibrium conditions, an invariant solid state transition will occur below 995 °C where the three-phase structure culminates in a phase assembly  $\beta/\gamma/\gamma'$ .  $\alpha$ -Cr +  $\beta$ -NiAl +  $\gamma$ -Ni will transform to  $\beta$ -NiAl +  $\gamma$ -Ni +  $\gamma'$ -Ni<sub>3</sub>Al. [10]. It should be noted that the phase transition in the eutectic alloy is associated with a linear shrinkage of about 0.5 % [10].

Disk-shaped coupons of  $\text{Ø}10 \times 1 \text{ mm}^2$  were wire spark-erosion cut from the alloy bar. The coupons got a smooth surface finish (1000 grit emery paper) prior to fastening them to a disc mounting sample holder via electron beam welding (Fig. 2). The sample holders serve both initially to position the samples during processing in the coater properly and also later on to ensure the rapid placing and removal on furnace testing. 20  $\mu\text{m}$  thick EBPVD 7YSZ top coats were applied on the coupons in a rotation mode at 1000 °C substrate temperature. The sequence of the temperature loadings is shown in Fig. 3.

The cross-sectional micrograph of the as-coated condition shows a 20  $\mu\text{m}$  thick 7YSZ top coat and a 0.2–0.3  $\mu\text{m}$  thick TGO interlayer. The substrate still shows  $\alpha$ ,  $\beta$  and  $\gamma$  phase which corresponds roughly to the initial structure of the substrate. The

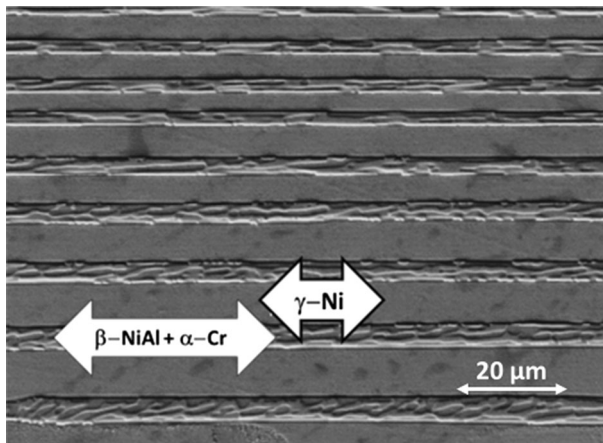


**Fig. 1** Aligned microstructure of as-solidified lamellar eutectic Ni–37.5Cr–7.0Al alloy showing narrow strips of interconnected  $\beta$ -NiAl– $\alpha$ -Cr phases sandwiched by broad  $\gamma$ -Ni lamellae (SEM secondary electron imaging mode). The structure represents the metastable state frozen in below the solid state transition temperature (995 °C) possibly retained because of the quenching effect during directional solidification processing under a high temperature gradient

**Table 1** EDS analysis of the phases in the as-solidified state in at.%

Phase	Ni	Cr	Al
$\alpha$ -Cr	37.80	46.38	18.82
$\beta$ -NiAl	60.07	10.68	29.25
$\gamma$ -Ni	59.27	32.96	7.87

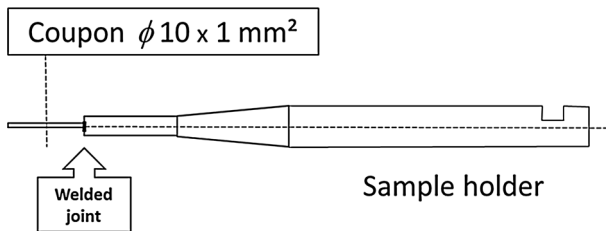


**Fig. 2** Coupon mounting sample holder used for EBPVD TBC processing of samples

substrate/TGO interface, which had been previously provided as a highly polished flat surface, shows now some unusual features in the composite structure; see Fig. 4. Supposedly they have formed during the 12 min hold time in the coater at 1000 °C operated in a low pressure regime of about  $10^{-5}$  atm. On top of some  $\alpha/\beta$  lamellae, local disconnections at the interface and the associated formation of cavities can be observed (see black arrows). These sites were not further examined. On top of some other lamellae about 1  $\mu\text{m}$ , high metallic hillocks have formed. They protrude from the alloy surface into the ceramic (see white circles); they show perfect adherence. In “TGO Formation on DS NiCrAl Bond Coat Surrogate TBC System,” section the behavior of the hillocks in the layer composite will be discussed.

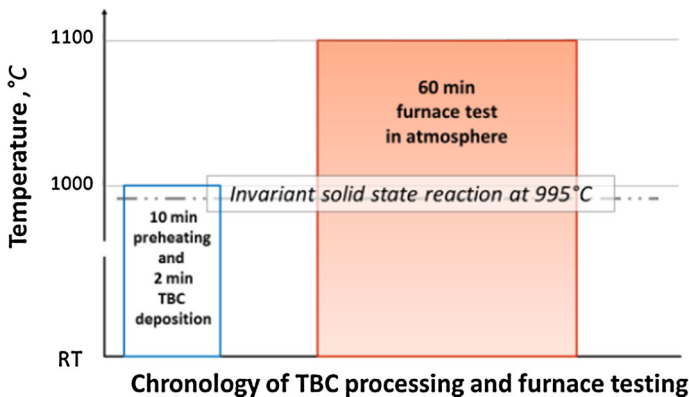


**Fig. 3** The sequence of the temperature loadings showing the respective operating temperatures which are all above the “critical” transition temperature of 995 °C

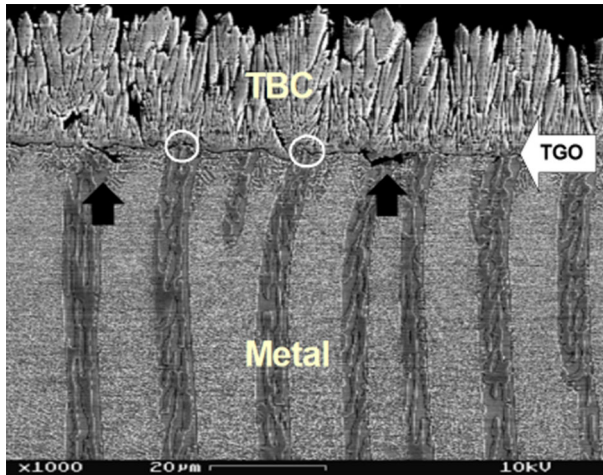


**Fig. 4** EBPVD processed condition of NiCrAl substrate resulting in a 20  $\mu\text{m}$  thick 7YSZ TBC and a 0.2–0.3  $\mu\text{m}$  thick TGO interlayer. Local detachment of the layer causes cavities at the top of some  $\alpha/\beta$  lamellae (indicated by *black arrows*). Some  $\beta/\alpha$  rows terminate at  $\sim 1 \mu\text{m}$  high hillocks (see *white circles*) protruding into the zirconia top coat

### SEM/EDS Microanalysis

Coupons were mounted in the upright position for the sake of a favorable vertical incidence inspection of the cross-section of the layered microstructures. The coupons were investigated and analyzed via EDS spot measurements by means of a SEM LEO Ultra 55, Zeiss Inc. Oberkochen, Germany, equipped with EDS Oxford Instruments, Oxfordshire, UK. The accelerating voltage was reduced for the purpose of a high spatial resolution. The reduction in accelerating voltage and concomitant drop in counting rate was compensated by an increase of measurement time to 30 min per site. The spot size has been pre-estimated via Monte Carlo simulation as a function of accelerating voltage and appropriate materials, see Table 2.

**Table 2** Calculation of the excited spot size on materials as a function of accelerating voltage

Material	Spot size accelerating voltage 4 kV ( $\mu\text{m}$ )	Spot size accelerating voltage 8 kV ( $\mu\text{m}$ )
ZrO <sub>2</sub>	0.15	0.3
Al <sub>2</sub> O <sub>3</sub>	0.5	1.5
Cr <sub>2</sub> O <sub>3</sub>	0.2	0.5
Ni	0.15	0.4
NiAl	0.3	0.9

## Results

### Lifetime Assessment and Relative Life

Lifetime estimates on the NiCrAl-based TBC coupons were derived from the exposures of four samples to 15, 30, 45 and 60 min, respectively, at 1100 °C in a furnace at atmosphere, followed by prompt air cooling to RT. First incipient spallation was observed after a 30 min interval at temperature. This appears as an about 3 mm long straight crack without bulging near the area of the sample edge. It is probably oriented to the lamellar structure of the substrate. This particular time up to failure is considered the actual lifetime which in the following is taken as a benchmark. In this sense, the four samples represent in turn a “relative life” of 50, 100, 150 and 200 %.

### Microstructure of Failed Sample Furnace-Tested at 1100 °C for 60 min

The sample for investigation has been subjected to the double relative lifetime (60 min at 1100 °C) according to the above definition of life. The TGO has now grown to a final thickness of about 0.5  $\mu\text{m}$ . The substrate shown in Fig. 5 at the very right represent the upper part of a similar type of a metallic hillock as has been highlighted before in white circles in Fig. 4.

They show complex changes in microstructure and phase assemblage. There is no  $\alpha$ -Cr phase any more. The former  $\alpha$ -Cr,  $\beta$ -NiAl, and  $\gamma$ -Ni phase mixture is transformed into a dual  $\beta/\gamma$  structure instead with some additional  $\gamma'$ -Ni<sub>3</sub>Al phase; the latter has been precipitated in a lamellar  $\gamma/\gamma'$  formation to be shown between the “offset particle” above at the rim of the crack and the  $\beta$ -phase area below in Fig. 5.

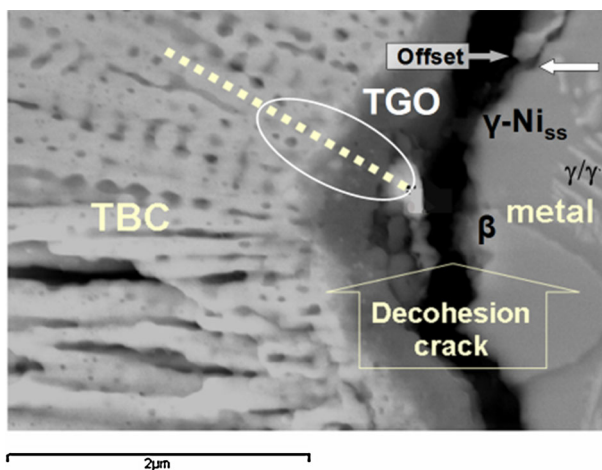


**Fig. 5** Failure site of Ni–Cr–Al/TBC sample due to Me/TGO separation on furnace anneal at 1100 °C for 60 min. Note that at this scale the MZ is not resolved. The *dotted line* between the bright particle in the crack zone and the interior zirconia layer represents the positions for EDS spot analysis; the data are compiled in Fig. 6

The sample displays the propagation of a separation crack of usually 0.2–0.5  $\mu\text{m}$  width running along the Me/TGO interface. It extends over broad ranges; most of it is completely chipped off. Crack propagation like this is typical of EBPVD TBC systems. However, at some locations the crack runs atypically over short distances in the hilltop areas in two respects which have never been observed in EBPVD systems before:

- (i) It deviates from the metal/scale interface and passes instead the metallic lamellar segment phase below in a serrated crack pattern. A metal piece remains adhered to the TGO (bright particle in the crack zone); the residual counterpart in the form of a lamellar segment now shows its serrated fracture surface.
- (ii) The piece of metal which has been separated by the crack propagation, adheres firmly to the TBC; the fracture surfaces on the metal piece and the left behind lamella segment match perfectly. The metal piece adhering to the TGO demonstrates longer-lasting adherence of the particular metallic phase to the TGO compared with the neighboring  $\gamma$  phases that could not keep adhesion to the TGO.

### Microanalysis via EDS Spot Measurements

The analyzed metal piece is most likely  $\beta$ , which is suggested by both the raised Al content as well as by the Gibbs phase rule: a three-component system contains no more than three phases; and these are  $\beta$ ,  $\gamma$  and  $\gamma'$ , where  $\beta$  is the Al-richest. But the data raises the question, why it displays this exceptionally high concentration of 20.6 at.%O. Presumably, it is partially due to subsurface material rather than the lateral spread of the beam to adjacent oxide regions. This case illustrates the operational limits of the SEM/EDS method in analyzing of small objects.

Comparing the analysis data of as-processed  $\beta$  (Table 1) with those of Table 3 allow the following statement: The Ni/Al ratio of about 2 in both the as-processed state and the metal piece are the same. The Ni/Cr ratio on the other side is different, namely 6 compared to 4. Hence, the type of question subsurface material is assumed to be Cr-rich oxide. The analysis data of the MZ is given in Table 4.

## Discussion

### Causes of Failure and Failure Mechanisms of EBPVD TBC Systems

In particular, undoped Al-forming alloys generate interfacial *voids alias pores at the metal/scale interface* as a result of extensive high temperature oxidation in air. The outward flux of cations in the scales necessitates an inward flux of vacancies—it is higher in undoped than in rare earth element doped scales. The vacancies agglomerate and promote the creation of pores via heterogeneous nucleation at the interface. The required nucleation energy for forming the pores is extremely



**Table 3** EDS spot analysis of the bright metal particle shown in Fig. 5 at the edge of the white marked ellipse at the far right

Element	At. %
Ni	44.99
Cr	11.02
Al	23.39
O	20.60

**Table 4** EDS spot analysis of MZ

Element	At. %
Cr	20.59
Ni	0.91
Al	14.82
Zr	4.38
Y	0.86
O	58.41

sensitive to changes of the surface energy [11]. The energy term is influenced by the surface morphology. The local vapor pressure is inversely related to the radius of curvature at interface unevenness. The energy increase at these irregularities causes inter alia a locally increased vapor pressure which compromises the adhesion strength and leads to blistering. Hence, the process of heterogeneous nucleation of pores at interfaces is not only facilitated or accelerated by a higher concentration of vacancies, but essentially by a rough and jagged metal/scale interface. The reduced adhesion strength of the metal/scale interface will sooner or later shorten the service life of TBC systems. Pores are furthermore stabilized by the presence of sulfur and more so with further thickening of the substrate [12]. Sulfur segregates readily to interfaces and surfaces thereby stabilizing the pore walls [13, 14], and thus causing premature interface separation failure [15].

The *failure* of NiCoCrAlY bond coated EBPVD TBC systems starts always by separation crack propagation at the scale/metal interface as mentioned before. The former  $\beta/\gamma$  bond coat on the outside in contact with the TGO has meanwhile transformed in service to single-phase  $\gamma$  due to extended selective oxidation of Al. Thus, separation of the scale from the metallic  $\gamma$  phase is generally found after extended thermal fatigue of typical EBPVD TBC systems. Except for the  $\gamma$ , there is no further metallic phase any more, which would still hold an Al-reservoir.

The *thickness of EBPVD TBC top layers* has no significant effect on life. The columnar structure of the TBC prevents the formation of compressive stresses; the in-plane Young's modulus is almost zero [16]. The thin scale only dominates the stress scenario in the layer composite. Hence, the thickness of the columnar ceramic topcoat is no life-determining factor.

Unlike PVD NiCoCrAlY bond coated TBC systems, the systems with either PS or NiPtAl bond coats respond sensitively to changes in the cycle length on thermal fatigue. The causes for the *frequency dependence of the lifetime* for the latter TBCs are quite complex. One main reason is seen in the compressive stresses within the

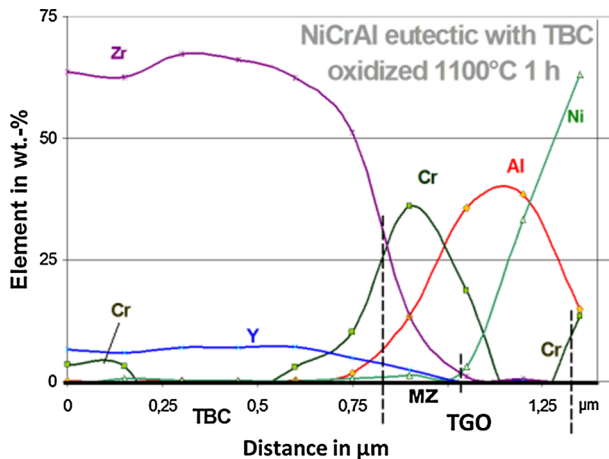


**Fig. 6** EDS line profile from rung region in Fig. 5. The Zr- and Al-profiles clearly indicate the existence of a  $ZrO_2/Al_2O_3$  mixed zone in the upper TGO layer which in this case exhibits an additional Cr enrichment. The lower TGO section at the *bottom* shows an increased Ni content attributable to the adhering metal piece (EDS data see Table 3)

scale in which the metal/scale interface is uneven and curvaceous. Here the scales grow to be wavy (rumpling). On their buckles, cracks may occur at the interface (buckling) and on the flanks shear cracks are initiated. The latter grow under cyclic thermal loading (wedging) [17]. Such mechanisms are not typical of the failure of EBPVD TBC systems. As an exception to this rule, the rumpling for the EBPVD TBC system IN617/NiCoCrAlY/YSZ was observed during isothermal aging at 1100 °C. The sample failed by wedging on the flanks of the buckles [18]. Perhaps, the characteristic flatness of the scale/metal interface of this particular EBPVD TBC system could not be maintained permanently, as the substrate is a forge alloy being less suitable for stabilizing the interlayer constantly in its in-plane orientation.

Another exception to the norm is represented by the extension of the service life under extremely short thermal load cycles. Stress relief processes are mentioned to be responsible for the expanded lives under the rapid thermal cycling conditions [4]. Perhaps, the short periods at high temperatures are ineffective to cause the nucleation of voids and pores adjacent to the interface for lack of accumulated vacancy clusters. There are too few pores growing, to weaken the adhesion substantially.

The life is hardly affected by the CTE misfit ratio. In this respect Fig. 7 is to be understood that—despite all logical arguments—the PVD variants showing the highest CTE mismatch demonstrate the longest life. Consequently, the service life is less determined by mechanical quantities such as the CTE, but rather by causes of a chemical nature.

### TGO Formation on DS NiCrAl Bond Coat Surrogate TBC System

The shape of the TGO within this particular TBC system is not typical for EBPVD TBC system which commonly grows even and parallel to the metal/TBC interface.

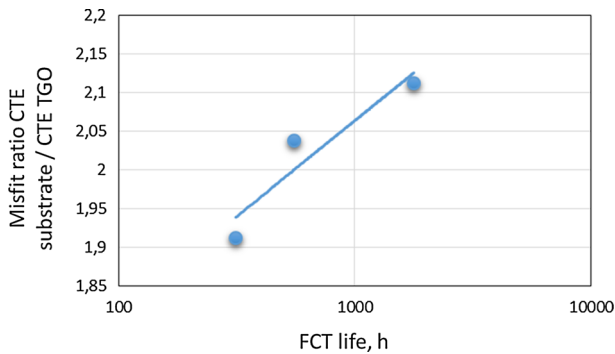


**Fig. 7** CTE mismatch ratio (RT...1000 °C) versus the average life (log scale) on three cyclic furnace tested (1100 °C) EBPVD TBC systems. Their substrates/lives: IN100 (660 h), CMSX-4 (376 h), MCrAlY (2132 h) [19]

Instead, this one shows an uncommon shape of growth exhibiting occasional bulges or “hillocks”. To better understand these different formations, some manufacturing steps are explained in more detail. Conventional NiCoCrAlY bond coat alloys are vapor-deposited on smoothly prepared workpieces. Subsequently, the homogeneous but porous NiCoCrAlY layer is ball-peened to densify and flatten it. The deformation stresses generated during peening are then resolved by a vacuum anneal at 1080 °C. The obtained  $\gamma/\beta$  layers show metallic luster with small YAG precipitates on it. This surface is ready for reactive vapor deposition with YSZ at 1000° C. In this procedure, the TGO grows. The buckling and rumpling of scales which is specially reported to occur for PS- and NiPtAl bond coated TBC systems [18] is noticeable only subsequent to thermal loadings.

The DS bond coat surrogate does not necessarily require these treatments. However, it has been considered before deciding on the waiving of a heat treatment, if a suitable heat treatment below the solid state reaction is to be performed. Thereby, the  $\gamma/\beta$  phases would have been stabilized at <995 °C, and the reaction-induced shrinkage and associated tension problems would have been bypassed. This project has been postponed. Accordingly, it has been taken into account that the suspected volume shrinkage yields an additional insight.

The DS substrate has already got a 1000 grit finish, and it is expected to be in a tension-free state. It has no YAG precipitates, since it is undoped. The following reactive vapor deposition of YSZ (1000 °C) results in the final shape of the TGO. Several hillocks have been grown efficiently, and thus uplifted the former flat metal/TBC interface (see white circles in Fig. 5). The local bulge is restricted on several  $\alpha/\beta$  lamellae. For the purpose of protruding into the ceramic layer two mechanisms must complement each other.

- (i) Convoluted scales are produced by the scale growth process with significant contribution from outward diffusion of cations as suggested by [20]. Notably, substantial outward diffusion is indirectly confirmed by the high Cr content in the actual TGO. In particular, compressive stresses arise in the

- TGO from the volume expansion as new oxide is internally formed; these cause lateral growth of the scale leading to rumpling and sliding at the alloy/scale interface. A similar mechanism of lateral growth is impressively reported on bcc Fe–28 %Cr–4 %Al alloy having <5 ppm sulfur: an oxidizing sheet sample formed a convoluted protective scale. By contrast, a particularly thin foil of this alloy generated in-plane even scales, wherein, however, this sample has lengthened by several percent on oxidation [21].
- (ii) The substrate must be capable to deform easily and be very low in sulfur to prevent the loss of contact to the scale [21]. In NiCrAl alloys, the fcc phases like  $\gamma$  are much more creep resistant at temperatures than the bcc phases  $\beta$  and  $\alpha$ -Cr. Therefore, the formation of scale protrusions on this low sulfur multiphase material is restricted on the  $\alpha/\beta$  lamellae. Thus, hillocks have been formed there where they have adapted to the conditions of lateral TGO growth and local plasticity of the substrate.

### High Temperature Oxidation-Tested DS NiCrAl Bond Coat Surrogate TBC System

A particularly rapid transformation of the quickly growing sub-oxides into stable oxide presumably occurs in the MZ due to the high inner Cr content (see Table 4). The peak temperatures for solid-state conversion of high temperature Cr-rich corundum in its two isomorphous phases  $\text{Al}_2\text{O}_3$  and  $\text{Cr}_2\text{O}_3$  is given in the literature with 900 °C [22] to 1250 °C [23]. While there are various polymorphs of  $\text{Al}_2\text{O}_3$ , this is not the case for  $\alpha$ - $\text{Cr}_2\text{O}_3$ . There are no polymorphs. Probably the low thickness of the MZ of 0.25  $\mu\text{m}$  is due to this fact, e.g., by triggering a more rapid transient  $\rightarrow$  stable conversion to  $\alpha$  alumina by its isomorph to  $\alpha$  neighbor phase; noteworthy a typical MZ is approximately five times as thick [8].

The exceptional appearance of this separation crack in Fig. 5 contradicts the expectations that are based on the thermal fatigue related failure mechanisms of TBC systems. Agreed causes of separation failure are attributed to irregularities and convolutions of the metal/scale interface. They may act as mechanical crack initiators as well as interfacial crack initiation sites via heterogeneous nucleation of voids by vacancy injection at the most curved locations. The top of the hillock is regarded as such a special point for void formation and subsequent separation. The facts in the micrograph (Fig. 5), however, shows the opposite behavior. The scale has detached from the surrounding interfaces, but at the top of the hillock it adheres firmly to a metallic substrate phase. It is a  $\beta$ -phase particle sticking to the TGO which presumably has been pulled out from the substrate due to high tension stresses. The adhesion strength between the  $\beta$  particle and TGO exceeded the strength of the substrate, and in particular the  $\beta$ -phase. This situation is schematically highlighted in Fig. 8.

The image reveals decisive differences in the adhesion strength which occur between TGO and different equilibrium phases under the same boundary conditions. With respect to a thermodynamic perspective, the chemical potentials of different solid phases in a heterogeneous system are equal across phase boundaries. This

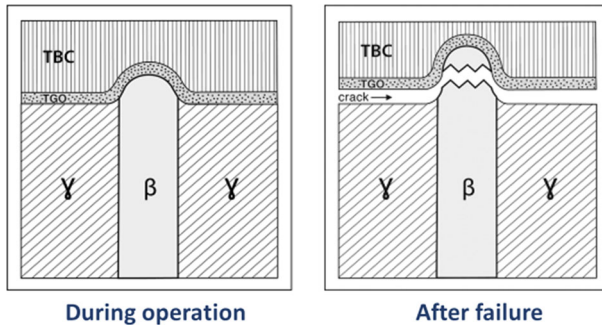


**Fig. 8** Schematic highlighting the tearing out process of some  $\beta$  particle from the DS NiCrAl substrate on furnace testing: The state during high temperature loading prior to TBC separation (left) is compared with the state after TBC disconnection while maintaining a remainder of  $\beta$  phase in the TBC (right)

statement is addressed in the Gibbs–Duhem equation:  $n_1 d\mu_1 + n_2 d\mu_2 = 0$ ,  $n$  refers to the respective number of moles and  $\mu$  to the associated chemical potential. The chemical potential includes the activity of the individual components, including the activity of oxygen. Oxygen is an essential part of the adhering scale, and therefore with  $\beta$  and  $\gamma$  in equilibrium. The further procedure is led by tracing the cause of the differences in the oxygen potentials of TBC systems. Hence, the following “[High Temperature Oxidation-Tested DS NiCrAl Bond Coat Surrogate TBC System](#)” and “[Oxygen Potentials in TBC Systems Ranging from the Atmosphere to the Substrate](#)” sections are intended to give an idea to the chemical oxygen potential across a TBC system, and then to the oxygen potential of the individual phases in a ternary  $\beta$ – $\gamma$ – $\text{Al}_2\text{O}_3$  phase diagram.

The high tensile stresses arise from at least two sources: one is the contraction according the CTE of the alloy during cooling, and the other, a potentially more significant solid state reaction. It causes an associated linear contraction of  $\sim 0.5\%$  as evaluated in cast eutectic material [10]. The shrinkage is mainly due to the smaller molar volume of the close-packed fcc  $\gamma/\gamma'$  phases at low temperature as compared to the body-centered cubic  $\alpha$ -Cr/ $\beta$ -NiAl at high temperatures. The off-plane orientation of the tensile stress could be due to the alignment of the former narrow strips of interconnected  $\beta$ -NiAl– $\alpha$ -Cr phases within the broad  $\gamma$ -Ni lamellae (see Fig. 1).

The rapidly shrunken alloy volume within the hillock tries to tear apart the scale/alloy interface. But the adhesion forces between the  $\beta$  particle and TGO proved stronger than the  $\beta$  substrate. The  $\beta$  is even weaker than the opposing ceramic layers. Perhaps, it is the stable “architecture” of the bulged scale/TBC composite layer that can withstand the tension stresses.

In this context, the formation of similarly organized shear stresses can be assumed for the offset structure in Fig. 5. It reflects their effects onto the metal/TGO interface at the shoulder-like part of the hillock. The shear stresses are induced there due to the solid state reaction that generates the close-packed fcc  $\gamma/\gamma'$  structure at the expense of some former voluminous bcc portions. In this conflict between still adhering metal and volume shrinkage in the underlying substrate the offset particle

could thus have been displaced. This mechanism only works if the volume shrinkage takes place chronologically before the local separation at the scale/metal interface. So, the volume shrinkage takes place first, during which the metal/TGO adhesion is still acting and opposes the shear stresses.

The very short life of this model system raises some questions. One refers to the sulfur content of the substrate. As is known, S accumulates quickly in boundary layers and causes separation there [12]. These requirements for low sulfur and low thickness of the substrate have been carefully satisfied. In addition, it does not contain rare earth elements, which would prolong life.

The lifetime of  $\frac{1}{2}$  h at 1100 °C brought about for the ternary NiCrAl TBC sample in this study is in line with the one reported for undoped binary NiAl samples of Ni<sub>60</sub>Al<sub>40</sub> composition of 1 h at 1100 °C. It is sub-stoichiometric  $\beta$  phase [24]. The ternary  $\beta$  phase in this study is sub-stoichiometric likewise, resembling the  $\beta$  phase composition Ni<sub>60</sub>Cr<sub>11</sub>Al<sub>29</sub> implied in Table 1. For that reason, a roughly comparable short life was to be supposed.

### Oxygen Potentials in TBC Systems Ranging from the Atmosphere to the Substrate

The oxygen potential gradient OPG is the driving force for outward diffusion of oxygen-active elements across the scale [25, 26]. The equilibrium partial pressures for oxygen  $p_{O_2}$  with alloys containing these elements requires a very low partial pressure of O<sub>2</sub> at the scale/metal interface. Assuming thermodynamic equilibrium at an Al<sub>2</sub>O<sub>3</sub>/alloy interface, the  $p_{O_2}$  there would be the dissociation pressure of Al<sub>2</sub>O<sub>3</sub> at the oxidation temperature. At 1100 °C, the  $p_{O_2}$  for Al<sub>2</sub>O<sub>3</sub>/ $\gamma$ -phase is about  $10^{-26}$  atm [27]. Lower  $p_{O_2}$  within the metal are displayed in the case that higher Al contents are concerned, e.g., at the Al<sub>2</sub>O<sub>3</sub>/ $\beta$  interface of about  $10^{-27}$  atm.

It was concluded on the basis of kinetic experiments on EBPVD TBC systems at high temperatures that the MZ is not protective [29]. This indirect evidence of atmosphere within the MZ during oxidation experiments has been affirmed by a “test reagent”; the slight vanadium content of IN100 substrate acting as an indicator for a high oxygen potential in the MZ of this TBC system [30] resulted in the precipitation of YVO<sub>4</sub> at the MZ/lower TGO interface. This compound ( $M_S$ : 1810 °C) is only stable in atmosphere and would decompose at a lower  $p_{O_2}$  [31]. It confirms the presence of atmosphere across the total MZ. It is incorporated in a schematic drawing in Fig. 9. The drawing represents the oxygen potential gradient of a full-grown TBC system.

### Ni–Al–O Phase Diagram Showing the Equilibrium Oxygen Potentials for $\beta$ and $\gamma$

The findings of the complete separation at TGO/ $\gamma$  interphases and simultaneous partial adhesion at TGO/ $\beta$  will be interpreted via phase stability in the ternary Al–Ni–O at 1100 °C. It shall represent the states of the quaternary Al–Cr–Ni–O system in a simplified form, see Fig. 10. It includes the equilibrium partial pressures for

**Fig. 9** Variation of the oxygen chemical potential  $\mu_O$  versus the position within TBC cross-section (schematic). The oxygen potential gradient across the lower TGO section refers to log format [28]

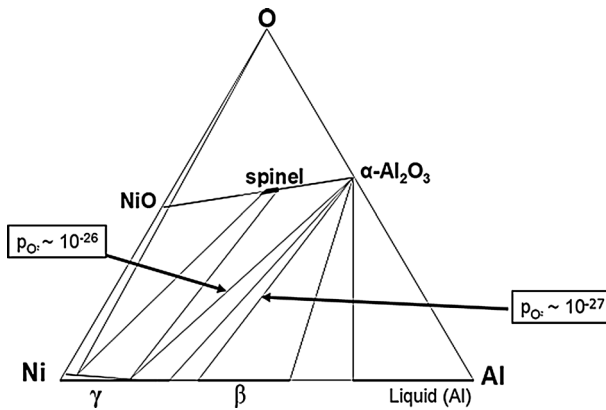
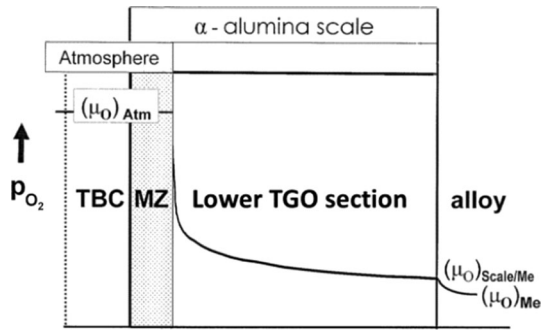


**Fig. 10** Schematic Ni–Al–O phase diagram for 1100 °C highlighting the equilibrium dissociation pressure for oxygen of  $\text{Al}_2\text{O}_3$  with  $\beta$  and  $\gamma$  phase [22, 27, 32–34]

oxygen [22, 27, 32–34] highlighting there  $p_{\text{O}_2} = 10^{-27}$  atm for sub-stoichiometric  $\beta$ -NiAl/TGO and  $10^{-26}$  atm for  $\gamma$ -Ni/TGO at this temperature. The difference between the set oxygen potentials is about an order of magnitude. Any rise in oxygen pressure, however, will compromise the chemical equilibrium at these locations necessary for selective oxidation of Al. Even a slight increase in oxygen pressure above  $10^{-26}$  atm will put the thermodynamic stability of the  $\gamma$ -Ni/TGO interface at risk upon stabilizing the bordering three-phase region  $\gamma + \text{Al}_2\text{O}_3 + \text{spinel}$ . At the same time, while the  $\gamma$ -phase is entering the critical three-phase region, the  $\beta$ -NiAl/ $\text{Al}_2\text{O}_3$  equilibrium is still at a slightly lower oxygen partial pressure where no potential spinel formation under equilibrium conditions can be expected.

It is a crucial criterion for good scale adhesion in Ni base alumina formers to avoid spinel phase at the scale/alloy interface [22]. To maintain the claimed low oxygen potential a sufficient Al-reservoir is supposed to be mandatory at the metal/scale interface. The reserve of sufficient  $\beta$ -phase in the bond coat would be beneficial. It should be recalled that TBC systems with NiCoCrAlY bond coats

**Table 5** Times at temperature (hot hours at 1100 °C), related relative lifetime (highlighted in bold), mid thicknesses of the MZ, EDS composition of the MZ of the DS NiCrAl/YSZ system from this study as compared to three NiCoCrAlY bond coated substrate/YSZ TBC systems from a previous study [8]

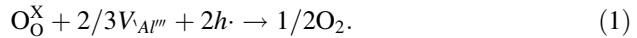
TBC system	Hot hours/relative lifetime	Cr	Y	Zr	Other elements	Y + Zr	Size of the MZ ( $\mu\text{m}$ )
Bond coat surrogate							
Ni–Cr–Al/YSZ	1	20.59	0.86	4.38	0.91 Ni	<b>5.24</b>	0.25
	<b>2</b>						
Conventional bond coat							
IN100/NiCoCrAlY/YSZ	417	0.45 $\pm$ 0.04	1.58 $\pm$ 0.47	1.49 $\pm$ 0.61	<0.2Co $\leq$ 0.15V	<b>3.07</b>	1.2
	<b>0.758</b>						
CMSX-4/NiCoCrAlY/YSZ	417	0.22 $\pm$ 0.09	1.64 $\pm$ 0.45	2.58 $\pm$ 0.42		<b>4.22</b>	1.2
	<b>1.33</b>						
MCrAlY/NiCoCrAlY/YSZ	417	0.21 $\pm$ 0.10	0.96 $\pm$ 0.38	0.84 $\pm$ 0.33		<b>1.80</b>	1.2
	<b>0.325</b>						

EDS data refer to Cr, Y and Zr and other elements of the MZ (at.%, balance is Al and O). The sum of the Y + Zr content is stated separately (in bold)



never show any contact of the  $\beta$  phase to the TGO at the end of life because their excessive lifetimes.

The differences in  $p_{O_2}$ , which have been shown to exist between  $Al_2O_3/\beta$  and  $Al_2O_3/\gamma$  will be linked to the dominant sub-step of oxidation occurring at the Me/TGO interface [28]. It is this exclusive site which is typical for separation failure of EBPVD TBC systems. The sub-step in Vink notation for semiconducting alumina lattice of presupposed Schottky-type—it stands for vacancy migration of point defects in ion lattices—is to be



The mass law for the reaction gives an equilibrium reaction constant  $K^*$  where the square brackets indicate concentrations, molar proportions or chemical activities of point defects giving

$$K^* = p_{O_2} / ([V_{Al}''']^{2/3} [h \cdot]^2 [O_O^X]) \quad (2)$$

According to the mass law, the deeper  $p_{O_2}$  regime results in some lower concentration of Al vacancies (and electron holes  $h \cdot$ ) aside from countercurrent oxygen  $O_O^X$ . That instance results in lower oxidation rates above all, due to the provision of less Al vacancies  $V_{Al}'''$ . This effect could not be experimentally investigated in this study. Notably lower oxidation rates are reported for alloys which are doped with reactive elements like Y as is well known [35]. These elements segregating to the Me/TGO interfaces at high temperatures may form RE-rich interlayers, which cause a lower  $p_{O_2}$  regime at the Me/TGO interface. In fact, a corresponding value of  $10^{-28}$  atm is reported for a Y-doped nickel alloy [36]. Notably, the dissociation pressure of  $Y_2O_3$  at 1100 °C is at its lowest with about  $10^{-37}$  atm [27] to account for the “reactive element” effect (REE) in this way. The REE was patented first in 1937 [37]. Notably, alumina and yttria form one another several compounds: YAG is one of them to happen typically in and below the scales of TBC systems. Its dissociation pressure is at about  $10^{-28}$  atm, as reported similar for the Y-doped nickel alloy.

No reactive elements are indeed in the DS NiCrAl substrate, but a significant amount of Cr has diffused from there to the MZ. The formation of the TGO is the result of a mixed transport mechanism comprising outward cation diffusion and inward oxygen diffusion. Slower transport rates for cations, e.g., by provision of a lower  $p_{O_2}$  regime at the Me/TGO interface according to Eq. (2) are estimated to result in a change from mixed to inward-dominated mass diffusion which also applies commonly with alumina-forming alloys.

### Comparing Between a DS NiCrAl Bond Coat Surrogate TBC System and Conventional EBPVD TBC Systems

In comparing the model system and the conventional EBPVD TBC systems their different lifetimes are the most striking. The life of TBC systems without doping

with rare earths is substantially diminished, as demonstrated in this study by the short life of just  $\frac{1}{2}$  h for the model TBC system.

To explain the influence of rare earths attention was drawn to the oxygen potential-lowering effect insinuated in Eq. (2). Overlay bond coats in TBC systems contain rare earths such as yttrium as a dopant to provide long lifetimes. Thus, the effect of Y dopants on the service life of TBC systems is positive.

Prior work [8] on conventional Ni base TBC systems coated with EBPVD NiCoCrAlY bond coats was focused on determining the service life by thermal fatigue tests and their scatter. The alloys to be examined were three alumina formers. They differ primarily in their content of refractory elements as Mo, Re, Ta, and W. The total refractory element content ranges from zero to 5.5 at.%. An approximate estimate of the relationship between TBC life and refractory element content in the substrates indicated the higher the content of refractory elements, the shorter the service life. Thus, the alloying of PVD NiCoCrAlY bond coated TBC systems with refractory elements has a detrimental effect on the service life with more increasing refractory element content. This behavior cannot be explained with the oxygen potential-lowering effect given in Eq. (2). Here are other reasons for this counteracting effect. These have been traced by analyzing the TGO via EDS.

TGO investigations revealed no traces of these refractory elements. Instead increasing levels of Y and Zr were found in the MZ. Their quantity has increased depending on the particular substrate and the time at temperature (see Table 5). A higher content of one of the two elements either Y or Zr is balanced by a lower content of the other. The sum of the two elements has proved to be decisive. The agglomeration rate of them in the MZ depends on the “relative lifetime” (it is the portion of lifetime as defined in “Lifetime Assessment and Relative Life” section).

If the relative life is taken as a reference, a universal relationship for the conventional EBPVD TBC systems investigated so far is evident [8]. The relationship

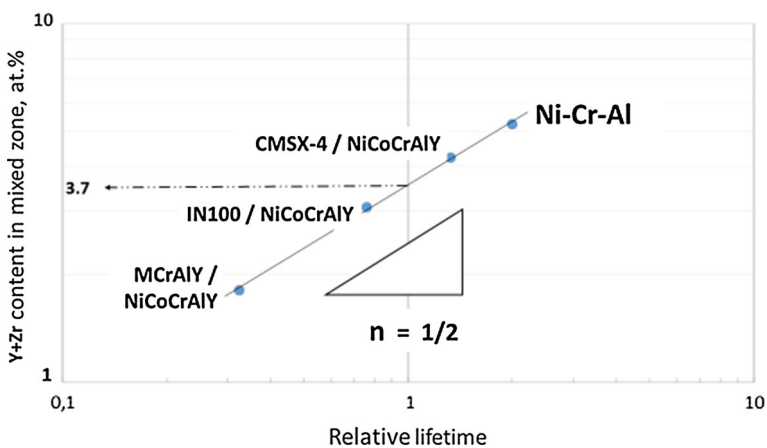


**Fig. 11** Y + Zr content in at.% in the MZ versus relative lifetime of NiCoCrAlY bond coated TBC systems and DS NiCrAl bond coat surrogate TBC system (double-log scale). 100 % of lifetime correlate with 3.7 at.% Y + Zr. The best-fit line follows a square root parabola relationship

will now be applied to the DC NiCrAl bond coat surrogate TBC system. It obviously applies to both the above-mentioned groups as shown in Fig. 11 (see related data in Table 5). The end of life (=1 alias 100 % of life) is indicated by a Y + Zr content of 3.7 at.%. The lives of the systems having PVD NiCoCrAlY bond coats as well as NiCrAl bond coat surrogates are determined equally alike by the sum of the Y and Zr content in the mixed zone.

The relationship cannot be interpreted with the scope of this paper. The square root relationship between relative life and Y + Zr content in the MZ is obvious. It suggests diffusion controlled processes which will be discussed in a subsequent paper.

## Summary

A directionally solidified NiCrAl ternary eutectic was provided to serve as a bond coat surrogate in an EBPVD 7YSZ thermal barrier coating system. The system was subjected to a furnace anneal, to determine the spalling of the ceramic layers or the adhesion of layer residues with respect to the phases of the alloy involved. The following statements can be deduced from the pilot experiment carried out:

- The alumina scale growth in the TBC systems changes from a mixed mode of the undoped NiCrAl alloy to an inward-oriented mode of conventional RE-doped alumina-forming systems.
- The transformation of growing up transition oxides into stable alumina is faster in the TBC system that has mixed mode diffusion.
- The growth mode and the growth rate of the scales are associated to the dissociation pressure of oxygen at the metal/TGO interface. Based on this pretention, the life of the TBC systems and the so-called “RE effect” are interpreted.
- The adhesion of the layers in EBPVD 7YSZ TBC systems and the life are attributable to chemical aspects. This is true both for conventional NiCoCrAlY bond coated TBC systems as well as for those with a NiCrAl bond coat surrogate. The sum of the Y and Zr content in the mixed zone interlayer is a lifetime-determining value.

**Acknowledgments** The authors would like to thank Wolfgang Braue for insightful discussions and comprehensive proofreading of the paper, Philipp Watermeyer for Monte Carlo simulations, and Eberhard Marx for graphic work.

## References

1. U. Schulz, K. Fritscher, U. Kaden, H. Lau, C. Leyens, and H.-J. Rätzer-Scheibe, in *International Symposium TurboMat 2002* (Wissenschaftszentrum Bonn, Bonn, 2002), pp. 44–47.
2. U. Schulz, M. Menzbach, C. Leyens and Y. Q. Yang, *Surface & Coatings Technology* **146–147**, (117–123) 2001.

3. W. Braue, K. Fritscher, U. Schulz, C. Leyens and R. Wirth, *Materials Science Forum* **461–464**, (899–906) 2004.
4. N. M. Yanar, M. Helminiak, G. H. Meier and F. S. Pettit, *Metallurgical and Materials Transactions A* **42**, (905–921) 2011.
5. J. A. Ruud, A. Bartz, M. P. Borom and C. A. Johnson, *Journal of the American Ceramic Society* **84**, (1545–1552) 2001.
6. U. Kaden, Einfluss der Substratlegierung CMSX-4 auf die Lebensdauer eines EB-PVD-Wärmedämmschichtsystems, Dissertation, *Werkstoffwissenschaftliche Schriftenreihe*, Vol. **56** (RWTH Aachen, Aachen, 2003). ISBN 3-86310-094-X.
7. L. Wang, D. C. Li, J. S. Yang, F. Shao, X. H. Zhong, H. Y. Zhao, K. Yang, S. Y. Tao and Y. Wang, *Journal of the European Ceramic Society* **36**, (1313–1331) 2016.
8. K. Fritscher, W. Braue and U. Schulz, *Metallurgical and Materials Transactions A* **44**, (2070–2082) 2013.
9. K. Fritscher, *Journal of Crystal Growth* **250**, (546–557) 2003.
10. K. Fritscher, C. Leyens and U. Schulz, *Materials Science and Engineering A* **369**, (144–150) 2004.
11. M. Bobeth, M. Gutkin, W. Pompe and A. E. Romanov, *Physica status solidi* **165**, (165–184) 1998.
12. J. G. Smeggil, *Materials Science and Engineering* **87**, (261–265) 1987.
13. H. J. Grabke, D. Wiemer and H. Viehhaus, *Applied Surface Science* **47**, (243–250) 1991.
14. B. A. Pint, *Oxidation of Metals* **48**, (303–328) 1997.
15. A. W. Funkenbusch, J. G. Smeggil and N. S. Bornstein, *Metallurgical Transactions A* **16**, (1164–1166) 1985.
16. U. Kaden, C. Leyens, M. Peters, and W. A. Kaysser, Einfluß thermischer Beanspruchung auf Morphologie, Struktur und Spannungszustand von EB-PVD-Wärmedämmschichten. *Werkstoff-Woche '98, Band II, Werkstoffe für die Verfahrenstechnik*, eds R. Stauber (Wiley-VHC, Weinheim, 1998), pp. 485–490.
17. A. G. Evans, G. B. Crumley and R. E. Demaray, *Oxidation of Metals* **20**, (193–216) 1983.
18. C. Leyens, Ausfallursachen und Versagensmechanismen von Wärmedämmschichtsystemen: Einfluss chemischer, mikrostruktureller und mechanischer Faktoren. *BTU Cottbus, Vol. 1* (Shaker Verlag, Aachen, 2006).
19. K. Fritscher, unpublished results (2015).
20. F. A. Golightly, F. H. Stott and G. C. Wood, *Oxidation of Metals* **10**, (163–187) 1976.
21. C. Forest and J. H. Davidson, *Oxidation of Metals* **43**, (479–490) 1995.
22. P. P. Saltykov, O. Frabrichnaya, J. Golczewski and F. Aldinger, *Journal of Alloys and Compounds* **381**, (99–113) 2004.
23. T. M. Besmann, N. S. Kulkarni and K. E. Spear, *Journal of the American Ceramic Society* **89**, (638–644) 2006.
24. R. Molins, I. Rouzou and P. Hou, *Materials Science and Engineering* **454–455**, (80–88) 2007.
25. B. Pint, *Oxidation of Metals* **45**, (1–37) 1996.
26. B. A. Pint and K. L. More, *Journal of Materials Science* **44**, (1676–1686) 2009.
27. I. Barin, *Thermochemical Properties of Inorganic Substances*, (Springer, Berlin, 1973).
28. M. M. Wada, T. Matsudaira and S. Kitaoka, *Journal of the Ceramic Society of Japan* **119**, (832–839) 2011.
29. R. D. Jackson, M. P. Taylor and H. E. Evans, *Oxidation of Metals* **76**, (259–276) 2011.
30. W. Braue, *Phase Relationships and Defect Structure During Oxide Formation and Growth in NiCoCrAlY- and (Ni, Pt)Al-based TBC systems*. *GRC on High Temperature Corrosion, July 24-29, 2005*, (Colby-Sawyer College, New London, 2005).
31. K. K. Byrappa, B. Nirmala, K. M. Lokanatha Rai, and M. Yoshimura, in *Handbook of Crystal Growth Technology*, Chap. 10, eds. K. Byrappa (India) and T. Ohichi (Japan) (William Andrew Publication, New York, 2003), pp. 335–366.
32. F. A. Elrefaie and W. W. Smeltzer, *Journal of the Electrochemical Society* **128**, (2237–2242) 1981.
33. M. Backhaus-Ricoult, *Berichte der Bunsen-Gesellschaft für Physikalische Chemie* **90**, (684–690) 1986.
34. C.-G. Kuo, W. D. Jehng, S.-J. Hsieh and C.-C. Chen, *Journal of Alloys & Compounds* **480**, (299–305) 2009.
35. B. Pint, in *Proceedings of the John Stringer Symposium on High Temperature Corrosion*, (5–8 Nov. 2001), pp. 9–19.
36. J. Balmain and A. M. Huntz, *Oxidation of Metals* **46**, (213–234) 1996.
37. W.G. Griffiths and L. B. Pfeil, Improvement in Heat Resistant Alloys. UK Patent No. 459848 (1937).